The Astrophysical Journal, 806:65 (8pp), 2015 June 10 doi:10.1088/0004-637X/806/1/65

NUSTAR, *XMM-NEWTON*, AND *SUZAKU* OBSERVATIONS OF THE ULTRALUMINOUS X-RAY SOURCE HOLMBERG II X-1

D. J. Walton[1,2], M. J. Middleton[3], V. Rana[2], J. M. Miller[4], F. A. Harrison[2], A. C. Fabian[3], M. Bachetti[5,6], D. Barret[5,6], S. E. Boggs[7], F. E. Christensen[8], W. W. Craig[7], F. Fuerst[2], B. W. Grefenstette[2], C. J. Hailey[9], K. K. Madsen[2], D. Stern[1], and W. Zhang[10]
[1] Jet Propulsion Laboratory, California Institute of Technology, Pasadena, CA 91109, USA
[2] Space Radiation Laboratory, California Institute of Technology, Pasadena, CA 91125, USA
[3] Institute of Astronomy, University of Cambridge, Madingley Road, Cambridge CB3 0HA, UK
[4] Department of Astronomy, University of Michigan, 1085 S. University Ave., Ann Arbor, MI, 49109-1107, USA
[5] Universite de Toulouse; UPS-OMP; IRAP; Toulouse, France
[6] CNRS; IRAP; 9 Av. colonel Roche, BP 44346, F-31028 Toulouse cedex 4, France
[7] Space Sciences Laboratory, University of California, Berkeley, CA 94720, USA
[8] DTU Space, National Space Institute, Technical University of Denmark, Elektrovej 327, DK-2800 Lyngby, Denmark
[9] Columbia Astrophysics Laboratory, Columbia University, New York, NY 10027, USA
[10] NASA Goddard Space Flight Center, Greenbelt, MD 20771, USA
Received 2015 March 30; accepted 2015 April 24; published 2015 June 9

ABSTRACT

We present the first broadband 0.3–25.0 keV X-ray observations of the bright ultraluminous X-ray source (ULX) Holmberg II X-1, performed by *NuSTAR*, *XMM-Newton*, and *Suzaku* in 2013 September. The *NuSTAR* data provide the first observations of Holmberg II X-1 above 10 keV and reveal a very steep high-energy spectrum, similar to other ULXs observed by *NuSTAR* to date. These observations further demonstrate that ULXs exhibit spectral states that are not typically seen in Galactic black hole binaries. Comparison with other sources implies that Holmberg II X-1 accretes at a high fraction of its Eddington accretion rate and possibly exceeds it. The soft X-ray spectrum ($E < 10$ keV) appears to be dominated by two blackbody-like emission components, the hotter of which may be associated with an accretion disk. However, all simple disk models under-predict the *NuSTAR* data above ∼10 keV and require an additional emission component at the highest energies probed, implying the *NuSTAR* data does not fall away with a Wien spectrum. We investigate physical origins for such an additional high-energy emission component and favor a scenario in which the excess arises from Compton scattering in a hot corona of electrons with some properties similar to the very high state seen in Galactic binaries. The observed broadband 0.3–25.0 keV luminosity inferred from these epochs is $L_X = (8.1 \pm 0.1) \times 10^{39}$ erg s^{-1}, typical for Holmberg II X-1, with the majority of this flux (∼90%) emitted below 10 keV.

Key words: black hole physics – X-rays: binaries – X-rays: individual (Holmberg II X-1)

1. INTRODUCTION

Ultraluminous X-ray sources (ULXs) are off-nuclear point sources in external galaxies that radiate in excess of the Eddington limit for a $\sim 10\,M_\odot$ "stellar" black hole such as those found in Galactic black hole binary systems (BHBs; e.g., Orosz 2003), i.e., $L_X > 10^{39}$ erg s^{-1} (Roberts 2007; Feng & Soria 2011). These luminosities may result from either the presence of larger black holes than those observed in our own Galaxy (e.g., Miller et al. 2004; Zampieri & Roberts 2009) or from super-Eddington modes of accretion (e.g., Poutanen et al. 2007). The majority of ULXs only radiate marginally in excess of 10^{39} erg s^{-1} (Swartz et al. 2011; Walton et al. 2011b), and there is now a reasonable consensus that these sources likely represent a high luminosity extension of the stellar remnant BHB population (Liu et al. 2013; Middleton et al. 2013; Motch et al. 2014). The best candidates for black holes significantly more massive than Galactic BHBs are instead found among the brightest members of the ULX population, with luminosities $L_X > 10^{40}$ erg s^{-1} (e.g., Farrell et al. 2009; Sutton et al. 2012; Pasham et al. 2014). However, while the majority of origins considered for this high luminosity population have focused on accretion onto black holes, with good reason given the luminosities in question, we now know that one source that exhibits these luminosities (albeit transiently) is in fact a pulsar (Bachetti et al. 2014), further expanding the pool of plausible scenarios (see also King et al. 2001).

Holmberg II X-1 is a source of particular interest among the bright ($L_X > 10^{40}$ erg s^{-1}) ULX population. Although variable on moderate timescales (∼days–weeks and longer, e.g., Grisé et al. 2010), it persistently radiates at a luminosity of $L_X \sim 10^{40}$ erg s^{-1} and is known to display a cool thermal component which may evolve following the $L \propto T^4$ relation expected for stable blackbody emission (Feng & Kaaret 2009; Miller et al. 2013). If associated with a standard accretion disk that extends close to the black hole, this would imply the presence of a massive black hole. However, high signal-to-noise X-ray observations of Holmberg II X-1 show the presence of curvature in the ∼3–10 keV continuum, which is generally interpreted as a signature of high/super-Eddington accretion (Gladstone et al. 2009; Kajava et al. 2012; see also Motch et al. 2014), although definitive evidence that this represents a genuine spectral cutoff is currently lacking for Holmberg II X-1 owing to the limited bandpass previously available (Caballero-García & Fabian 2010; Walton et al. 2011a).

Beyond the X-ray regime, observations of Holmberg II X-1 at longer wavelengths have revealed an X-ray ionized nebula and emission from moderately ionized oxygen which, through photon counting arguments, confirm the extreme X-ray

Table 1
Details of the 2013 X-ray Observations of Holmberg II X-1 Considered in this Work

OBSID	Start Date	Good Exposure[a] (ks)
	NuSTAR	
30001031002/3	2013 Sep 09	111
30001031005	2013 Sep 17	111
	XMM-Newton	
0724810101	2013 Sep 09	5/8
0724810301	2013 Sep 17	6/9
	Suzaku	
708015010	2013 Sep 17	52
708015020	2013 Sep 27	49

[a] *XMM-Newton* exposures are listed for the EPIC-pn/MOS detectors.

luminosity and rule out strongly beamed emission, implying that X-ray flux is broadly isotropic (Berghea et al. 2010). In addition, radio observations have now revealed that Holmberg II X-1 repeatedly launches collimated jets (Cseh et al. 2014), making it the only confirmed ULX known to launch such outflows.

Here, we present the results from broadband X-ray observations of Holmberg II X-1 undertaken with the *NuSTAR* (Harrison et al. 2013), *XMM-Newton* (Jansen et al. 2001), and *Suzaku* (Mitsuda et al. 2007) observatories. The paper is structured as follows: in Section 2 we describe our observations and data reduction, in Section 3 we present our analysis of these data, and in Section 5 we discuss our results and draw conclusions.

2. OBSERVATIONS AND DATA REDUCTION

During 2013 September *NuSTAR* and *XMM-Newton* performed two coordinated observations of Holmberg II X-1, separated by ∼8 days. The *XMM-Newton* exposures were short owing to visibility limitations, but both were simultaneous with some portion of the longer *NuSTAR* observations, providing soft X-ray coverage down to ∼0.3 keV. *Suzaku* also performed two observations of Holmberg II X-1 in 2013 September, the first coordinated with the second *NuSTAR*+*XMM-Newton* observation, and the second ∼10 days later. The details of the observations performed in our 2013 campaign are given in Table 1 (although the first *NuSTAR* epoch is comprised of two OBSIDs, it is one continuous observation). For each mission, source products were extracted from circular regions (*NuSTAR*: radius ∼75″; *XMM-Newton*: ∼40″ for EPIC-pn, ∼50″ for EPIC-MOS; *Suzaku*: ∼230″), and the backgrounds were estimated from blank regions free of contaminating sources on the same detector as Holmberg II X-1.

2.1. NuSTAR

We reduced the *NuSTAR* data using the standard pipeline, NUPIPELINE, part of the *NuSTAR* Data Analysis Software (NUSTARDAS, v1.3.1; included in the HEASOFT distribution), with the *NuSTAR* instrumental calibration files from caldb v20140414. The unfiltered event files were cleaned with the standard depth correction, significantly reducing the internal high-energy background, and passages through the South Atlantic Anomaly were removed. Source spectra and instrumental responses were produced for each of the two focal plane modules (FPMA/B) using NUPRODUCTS. The FPMA and FPMB data each provide an independent detection up to ∼25 keV.

2.2. XMM-Newton

The *XMM-Newton* data reduction was carried out with the *XMM-Newton* Science Analysis System (SAS v13.5.0), following the standard prescription provided in the online guide.[11] Raw data files were cleaned using EPCHAIN and EMCHAIN for the EPIC-pn and EPIC-MOS detectors, respectively. Only single and double events were considered for EPIC-pn and single to quadruple events for EPIC-MOS. Periods of high background flares were excluded. Instrumental response files were generated with RMFGEN and ARFGEN. After performing the reduction separately for the two EPIC-MOS detectors, and confirming their consistency, these data were combined into a single spectrum using ADDASCASPEC. The *XMM-Newton* data are analyzed over the 0.3–10.0 keV energy range.

2.3. Suzaku

As we have high energy coverage from *NuSTAR*, we only use the data obtained with the XIS detectors and do not consider the non-imaging HXD PIN detector. We cleaned the unfiltered event files with the latest calibration and the standard screening criteria for each of the XIS CCDs (XIS0/1/3) and editing modes operated ($3\times3/5\times5$), using the latest HEASOFT package (v6.15) as recommended in the *Suzaku* Data Reduction Guide.[12] Instrumental responses were generated for each detector using XISRESP (with a medium resolution). Finally, after checking their consistency, the data from the front-illuminated detectors (XIS0/3) were combined using ADDASCASPEC. The front- and back-illuminated (FI and BI) data are analyzed over the 0.7–10.0 and 0.7–8.0 keV energy ranges, respectively.

3. INITIAL SPECTRAL ANALYSIS

The spectra obtained from each of the two *NuSTAR*+*XMM-Newton* observations are consistent with each other, as are the spectra from each of the two *Suzaku* observations; no significant spectral variability is observed among any of these epochs. Therefore, to simplify the analysis, we combine the data into time-averaged spectra, and model the *NuSTAR*, *XMM-Newton*, and *Suzaku* data simultaneously; the spectral agreement between *NuSTAR*, *XMM-Newton*, and *Suzaku* in their common 3–10 keV bandpass is known to be good to within ∼10% in absolute normalization and a few percent in spectral agreement (within errors, Madsen et al. 2015; see also Brenneman et al. 2014; Walton et al. 2013a, 2014). All spectral analysis is performed with XSPEC v12.8.1 (Arnaud 1996). The *XMM-Newton* and *Suzaku* data sets are rebinned to 50 counts per bin, while the *NuSTAR* data are rebinned to 100 counts per bin, owing to the larger relative contribution of the instrumental background at higher energies. The observed broadband X-ray spectrum is shown in Figure 1.

Some basic conclusions can immediately be drawn from visual inspection of this spectrum. The continuum above

[11] http://xmm.esac.esa.int/
[12] http://heasarc.gsfc.nasa.gov/docs/suzaku/analysis/

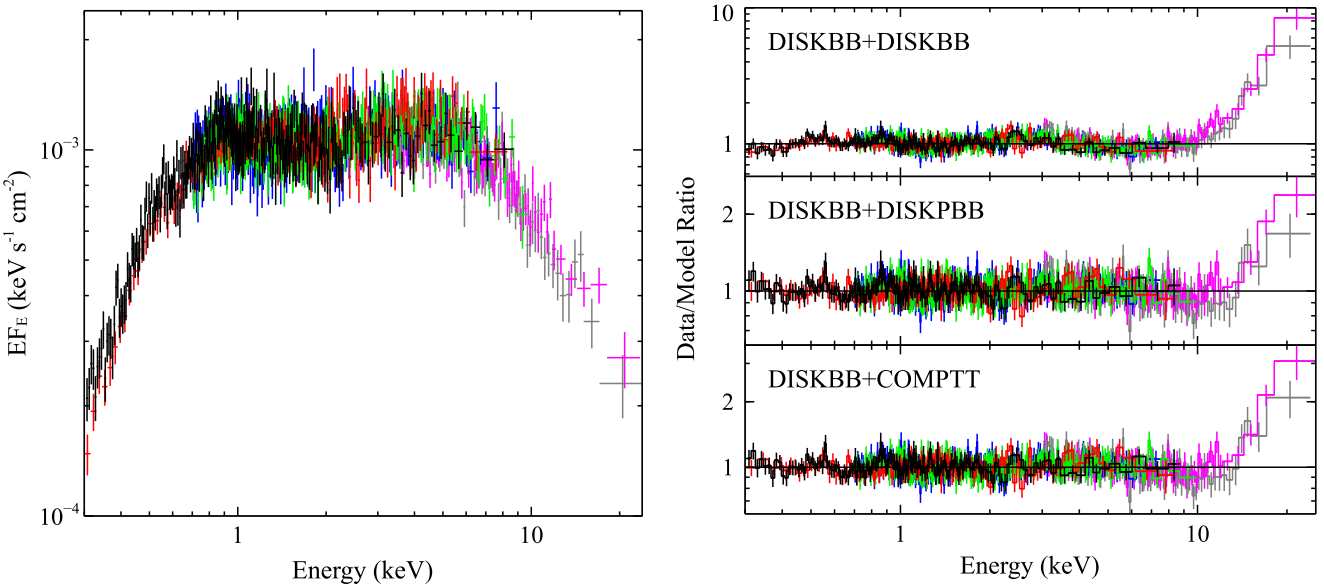

Figure 1. *Left panel:* the broadband X-ray spectrum of Holmberg II X-1, observed by *NuSTAR* (FPMA in magenta, FPMB in gray), *XMM-Newton* (EPIC-pn in black, EPIC-MOS in red) and *Suzaku* (FI XIS in green, BI XIS in blue) in 2013, unfolded through a model simply consisting of a constant. The *NuSTAR* data clearly demonstrate the presence of a high-energy spectral cutoff. *Right panel:* data/model ratios for the three two-component thermal continuum models considered. Each results in a clear excess in the residuals at high energies.

~2 keV is not power-law-like. The *NuSTAR* data clearly confirm the presence of the curvature in the ~3–10 keV bandpass claimed previously (e.g., Stobbart et al. 2006; Gladstone et al. 2009), and that this is a genuine spectral cutoff. This is broadly similar to other ULXs observed by *NuSTAR* to date (Bachetti et al. 2013; Walton et al. 2013a, 2014, 2015; Rana et al. 2015). Our analysis of these other sources has generally found that two blackbody-like thermal components are required to model their broadband spectra (see also Miller et al. 2014), and visual evidence for distinct spectral components above and below ~2 keV can also be seen here. We therefore focus on similar models in our analysis of Holmberg II X-1.

All subsequent models include neutral absorption from both the Galactic column toward Holmberg II ($N_{\rm H;Gal} = 3.7 \times 10^{20}$ cm^{-2}; Kalberla et al. 2005), and an intrinsic absorption column at the redshift of Holmberg II ($z = 0.002225$)[13] which is free to vary. Both are modeled with TBNEW (Wilms et al. 2000).[14] Unless stated otherwise, these absorption components are assumed to have solar abundances, and we adopt the abundance set in Wilms et al. (2000) and the cross-sections of Verner et al. (1996). Parameter uncertainties are quoted at 90% confidence for one parameter of interest throughout, and we account for residual cross-calibration flux uncertainties between different detectors by allowing multiplicative constants to float between them, fixing EPIC-pn to unity.

We begin by confirming quantitatively that two blackbody-like continuum components are required. Simple accretion disk models (e.g., DISKBB, Mitsuda et al. 1984; DISKPBB, Mineshige et al. 1994) cannot fit the broadband data by themselves, as they cannot reproduce the double-peaked spectral shape below 10 keV. We therefore apply models that include two continuum components, starting with a model consisting of two DISKBB components. However, the fit is poor, with χ^2/degrees of freedom (dof) = 2401/1899, and this model leaves a strong excess in the *NuSTAR* data above ~10 keV (see Figure 1). Although the fit is improved, this excess is not fully resolved by allowing the radial temperature profile of the hotter of the two disk components to vary (using DISKPBB; χ^2/dof = 1938/1898). Nor is it fully resolved by replacing the hotter disk component with a thermal Comptonization model (COMPTT; Titarchuk 1994), although the fit is again improved over the two DISKBB model (χ^2/dof = 1979/1898). For the Comptonization model, we link the seed photon temperature for the Comptonization to that of the lower temperature DISKBB component, as would be appropriate for standard, optically thin Comptonization. However, we find the corona to be cool and optically thick ($\tau \sim 6$; $T_{\rm in} \sim 2$ keV), similar to the results typically found for ULXs (e.g., Stobbart et al. 2006; Walton et al. 2011a). These parameters result in a disk-like spectrum with a thermal roll-over above ~5 keV. If the corona is optically thick and shrouds the inner disk, our assumption regarding the seed photon temperature may not be appropriate (e.g., Gladstone et al. 2009). However, even if we unlink this temperature from that of the DISKBB component, the hard excess still persists.

4. THE HARD EXCESS

Evidence for similar hard excesses has been seen in other *NuSTAR* observations of ULXs (e.g., Walton et al. 2013a, 2014; Mukherjee et al. 2015; Rana et al. 2015). However, for the cases that require complex thermal continua below ~10 keV (i.e., Holmberg IX X-1, IC 342 X-1 and NGC 5204 X-1) the significance of the excess is model dependent. Here, we find that a complex continuum consisting of two blackbody-like thermal components is required to model the spectrum below ~10 keV, and that a hard excess remains in the *NuSTAR* data above ~10 keV regardless of the details of this lower energy continuum. An additional high-energy continuum component is required by any model that falls away with a

[13] from the NASA Extragalactic Database: http://ned.ipac.caltech.edu/.
[14] http://pulsar.sternwarte.uni-erlangen.de/wilms/research/tbabs

Table 2
Key Parameters Obtained for the Three-component Continuum Models for Holmberg II X-1

Model Component	Parameter	Hard Continuum	
		Power-law	Bremsstrahlung
TBABS	$N_{\rm H}$ (10^{20} cm^{-2})	6^{+2}_{-1}	6^{+2}_{-1}
DISKBB	$T_{\rm in}$ (keV)	$0.20^{+0.03}_{-0.04}$	$0.23^{+0.01}_{-0.02}$
DISKPBB	$T_{\rm in}$ (keV)	$1.8^{+0.7}_{-0.3}$	$2.0^{+0.3}_{-0.2}$
	p	$0.67^{+0.10}_{-0.05}$	$0.55^{+0.03}_{-0.01}$
SIMPL	Γ	$3.1^{+0.3}_{-1.2}$	...
	$f_{\rm scat}$ (%)	40^{+50}_{-30}	...
BREMS	$T_{\rm brems}$ (keV)	...	12^{+32}_{-3}
χ^2/dof		1884/1896	1884/1896

thermal Wien tail. To address the nature of this hard excess, we focus on the best fitting two-component thermal model discussed above, the DISKBB+ DISKPBB combination.

To account for this hard excess, we first consider whether it might arise from an optically thin, hot Comptonizing corona such as found in Galactic BHBs. We add an additional high-energy power-law continuum using SIMPL (Steiner et al. 2009). This is a convolution model that scatters some fraction ($f_{\rm scat}$) of an input spectrum into a high-energy powerlaw tail with photon index Γ. We initially apply SIMPL to both disk components, such that each contributes the same powerlaw tail (i.e., Γ and $f_{\rm scat}$ are the same for each component). This would correspond to the "patchy disk" scenario outlined in Miller et al. (2014) (see discussion), in which the hotter and cooler emission regions are co-located, and thus the scattering medium likely subtends a similar solid angle for each. This gives an excellent fit to the broadband spectrum with χ^2/dof = 1884/1896, providing a statistical improvement of $\Delta\chi^2 = 54$ for two additional free parameters. The broadband 0.3–25.0 keV flux obtained with this model corresponds to an observed luminosity of $L_X = (8.1 \pm 0.1) \times 10^{39}$ erg s^{-1} for a distance of 3.39 Mpc (Karachentsev et al. 2002). Correcting for the neutral absorbing column inferred, the implied intrinsic 0.3–25.0 keV luminosity is $L_{X,\rm int} = (10.1 \pm 0.4) \times 10^{39}$ erg s^{-1}. Best fit model parameters are given in Table 2, and the fit is shown in Figure 2.

The SIMPL parameters are poorly constrained owing to the limited high-energy statistics, resulting in strong degeneracies. However, the best-fit photon index is steep, $\Gamma = 3.1^{+0.3}_{-1.2}$, similar to the coronae observed from Galactic binaries in the very-high state (Remillard & McClintock 2006). With the addition of this powerlaw continuum, we find that the radial temperature index obtained for the hotter (DISKPBB) component, $p = 0.67^{+0.10}_{-0.05}$, is consistent with that expected for a standard thin accretion disk ($p = 0.75$; Shakura & Sunyaev 1973). If we fix $p = 0.75$, the constraint on the photon index is significantly stronger: $\Gamma = 3.2^{+0.2}_{-0.1}$. We note that an equally good fit can be obtained assuming only to the (hotter) DISKPBB component is scattered into a high-energy tail. This would correspond to an alternative scenario in which the hotter and cooler emission regions are not co-spatial, but the cooler emission comes from much larger radii, and thus the scattering region, which is likely centrally located, does not intercept a significant fraction of this emission. The SIMPL parameters obtained are similarly poorly constrained and remain consistent with those presented, but in this case we find $p = 0.55 \pm 0.01$, significantly shallower than the thin disk case, closer instead to what might be expected from an accretion disk experiencing significant photon advection (e.g., Abramowicz et al. 1988).

An alternative possibility for the hard excess is that it is associated with the radio jets rather than with a Comptonizing corona. Several authors have suggested that SS433 might be a Galactic ULX analog, merely observed at a sufficiently high inclination that the X-ray emission from the central regions of the accretion flow is obscured from our view (Begelman et al. 2006). This source is also known to launch collimated jets, which themselves emit X-rays with a spectrum comprised of strong line emission (iron Kα equivalent width of ~350 eV) on top of a bremsstrahlung continuum (e.g., Marshall et al. 2002; Lopez et al. 2006). We therefore fit a model including a bremsstrahlung continuum for the hard excess to test an origin from SS433-like jet emission.

While the limits for any narrow iron features from these data are not as stringent as for other ULXs (e.g., Walton et al. 2013b), they are sufficient to exclude emission lines of the strength observed in SS433, with important implications for this jet emission model. We find that any narrow emission lines in the immediate 6–7 keV iron Kα bandpass must have equivalent widths less than 40 eV (at 90% confidence).

The metallicity of the system is a key issue relevant to the absence of strong jet lines in Holmberg II X-1. The dwarf galaxy Holmberg II appears to have a sub-solar metallicity in general, with an estimated metalicity of ~0.2 $Z_\odot$ (Egorov et al. 2013). A low metallicity could help hide any line emission. However, the low average metallicity of Holmberg II is not necessarily representative of the Holmberg II X-1 system, which may, for example, have been locally enriched by the supernova event in which the central compact object was formed. Should the excess absorption over the Galactic column along our line of sight to Holmberg II X-1 be largely local to the system, this would provide a better estimate of the relevant metallicity than looking at the galaxy as a whole. Unfortunately the lowest energies ($E < 0.7$ keV) of the broadband spectra obtained in our campaign, which are the most sensitive to the details of the absorption model, are only covered by the *XMM-Newton* observations, which were very short. These data are not able to provide any strong constraints on elemental abundances for the absorption intrinsic to Holmberg II, either individually or collectively; even assuming a consistent abundance relative to solar for all elements heaver than carbon we only find a weak upper limit of $Z < 1.8$ $Z_\odot$, although we note that the best-fit obtained with this approach implies a solar metallicity.

In their analysis of the longest *XMM-Newton* observation of Holmberg II X-1 available to date, Goad et al. (2006) suggest that the oxygen abundance of the absorbing medium toward Holmberg II X-1 might be sub-solar (O/solar ~0.6), based on the neutral oxygen edge at ~0.55 keV. However, this is estimated with a steep ($\Gamma = 2.6$) power-law continuum extrapolated to arbitrarily low energies, and our broadband observations show that the continuum is not a power law. This extrapolation likely results in the absorption column being overestimated, which would in turn lead to the oxygen abundance being underestimated in order to match the depth of the edge. Indeed, when these authors consider models in which the low-energy continuum is a disk blackbody, a solar abundance gives an improved fit over the sub-solar abundance inferred with the powerlaw continuum. Winter et al. (2007) also analyzed this data set with a view to constraining the

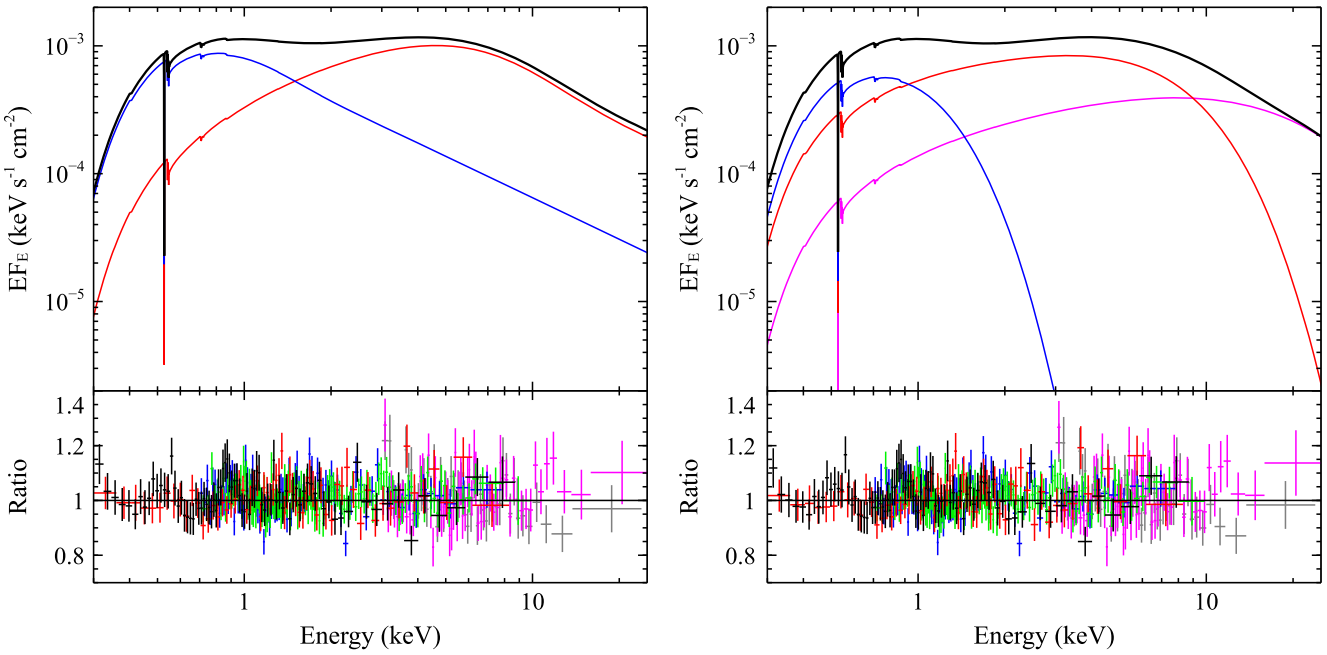

Figure 2. Fits to the broadband spectrum of Holmberg II X-1 with our three-component continuum models. The top panels show the models applied (black line); the base continuum model is a combination of DISKBB (blue) and DISKPBB (red) disk components, and the left panels show the hard excess modeled with a powerlaw tail (SIMPL), while the right panels show this excess modeled with bremsstrahlung emission (magenta). The bottom panels show their data/model ratios, with the same color scheme as Figure 1.

abundances of oxygen and iron, treating the soft emission both as a blackbody and a disk blackbody and typically found solar or slightly super-solar oxygen abundances depending on the exact model used (iron abundances were generally poorly constrained).

In contrast, Marshall et al. (2013) find that the outflowing material in the SS433 jets has a strongly super-solar metallicity of $\sim$6 $Z_{\odot}$. Although the metallicity of the Holmberg II X-1 system is ultimately still an open question, we therefore assume that for SS433-like jet emission, the iron lines would be a factor of $\sim$5–6 weaker relative to the bremsstrahlung continuum in Holmberg II X-1 than in SS433. However, given the limits discussed above and the lines observed from SS433, this difference by itself would not be sufficient to reduce the expected strength of these lines to the point that they would not be detectable with these observations of Holmberg II X-1.

We therefore conclude that the jet emission cannot dominate the continuum emission across the iron bandpass. When applying the bremsstrahlung model we therefore require that the bremsstrahlung flux is less than that of the hotter disk component at these energies. SS433-like jet lines would then be sufficiently diluted by this additional continuum emission to remain undetected, assuming the difference in metallicity discussed above. This provides an equally good fit to the powerlaw continuum, with χ^2/dof = 1884/1896; best-fit parameters for this model are also given in Table 2, and the fit is also shown in Figure 2. Similar to the coronal parameters in the previous model, the bremsstrahlung temperature is poorly constrained owing to remaining parameter degeneracies: $T_{\rm brems} = 12^{+32}_{-3}$ keV. In this case, we find $p = 0.55^{+0.03}_{-0.01}$ for the (hotter) DISKPBB component, again significantly shallower than the thin disk case.

5. DISCUSSION AND CONCLUSIONS

We have presented a broadband spectral analysis of the ULX Holmberg II X-1, observed with *NuSTAR*, *XMM-Newton*, and *Suzaku* in 2013, which provides the first constraints on the hard ($E > 10$ keV) X-ray emission from this source. These observations were taken at three epochs spanning a period of $\sim$3 weeks. We find no evidence for significant variability between them, and we therefore focus our analysis on the average spectrum. As with other ULXs observed with *NuSTAR*, we find clear evidence for a spectral cutoff above $\sim$5 keV (Figure 1; see Bachetti et al. 2013; Walton et al. 2013a, 2014, 2015; Rana et al. 2015), confirming the previous indication from archival *XMM-Newton* observations (e.g., Stobbart et al. 2006; Gladstone et al. 2009; Kajava et al. 2012). For comparison with previous observations, we note that $\sim$90% of the observed broadband luminosity ($L_X = (8.1 \pm 0.1) \times 10^{39}$ erg s^{-1}) is emitted below 10 keV, consistent with the typical range of fluxes for this source (Grisé et al. 2010).

The observed broadband spectrum is not consistent with the standard accretion states observed at low Eddington rates in Galactic binaries (Remillard & McClintock 2006). Under the assumption that these accretion regimes are mass-independent, this would imply that Holmberg II X-1 is accreting at a high fraction of its Eddington rate, and possibly exceeding it. Although this evidence is indirect, we note that the behavior of the best IMBH candidate to date, ESO 243-49 HLX1, suggests this is a reasonable assumption to make (Servillat et al. 2011). In additon, the spectrum of Holmberg II X-1 bears some broad similarity to the spectrum of the less luminous ULX P13 in NGC 7793 ($L_{X,\rm peak} \sim 5 \times 10^{39}$ erg s^{-1}). This source is notable, as the current dynamical mass constraints for P13 imply a mass of $\lesssim$15 $M_{\odot}$ for the accretor (Motch et al. 2014), indicating it is accreting at a high/super-Eddington rate. Holmberg II X-1 is

typically observed to be more luminous, which may imply a slightly larger Eddington ratio ($L/L_{\rm E}$) or a slightly elevated black hole mass in comparison to P13. Most models for strong super-Eddington accretion invoke thick accretion disks, resulting in some level of anisotropic emission with larger scale heights and therefore increasing levels of anisotropy at higher accretion rates (e.g., King et al. 2001; Dotan & Shaviv 2011). In principle, the roughly isotropic emission implied by the ionized nebula surrounding Holmberg II X-1 may therefore imply some upper limit to $L/L_{\rm E}$. However, the uncertain solid angle subtended by the nebula, which appears to exhibit some mild anisotropy (e.g., Kaaret et al. 2004), likely still allows for some moderate geometrical beaming, so unfortunately it is difficult to be quantitative here.

The spectrum below 10 keV shows evidence for two blackbody-like thermal continuum components. However, the Wien tail in all such models falls away faster than the high-energy data, resulting in a clear excess in the residuals above ∼10 keV. These models therefore require an additional, high-energy spectral component. Similar excesses have been seen in other ULXs observed by *NuSTAR* (Walton et al. 2013a), but for the cases where the lower energy spectrum is complex the requirement for an additional component was model dependent (e.g., Walton et al. 2014; Mukherjee et al. 2015; Rana et al. 2015). That is not the case here, despite the requirement for a two-component continuum model for the soft X-ray spectrum. This excess can be modeled successfully with an additional steep power-law tail, consistent with an optically thin Comptonizing corona. It can also formally be modeled with a hot bremsstrahlung continuum potentially associated with emission from the radio jets (Cseh et al. 2014), analogous to that seen from the jets in SS433 (Marshall et al. 2002, 2013).

In the jet emission model, we find the 2–10 keV luminosity associated with the bremsstrahlung component to be $L_{\rm brems} = (1.4 \pm 1.0) \times 10^{39}$ erg s^{-1} (the upper limit being a result of our requirement that this component be fainter than the DISKPBB component in the immediate iron bandpass; see Section 4), ∼3 orders of magnitude or more in excess of the jet emission observed from SS433 ($L_{\rm brems} \sim 3 \times 10^{35}$ erg s^{-1}; Marshall et al. 2002). The bremsstrahlung emission may scale with the radiative power of the jet. However, the core radio luminosity (L_R) is ∼2 orders of magnitude greater in Holmberg II X-1 than in SS433 (Miller-Jones et al. 2008; Cseh et al. 2014), implying that $L_{\rm brems}/L_R$ is at least an order of magnitude greater in Holmberg II X-1 than in SS433. While there is the obvious caveat that we are not comparing simultaneous radio and X-ray observations, the observed X-ray flux during this epoch is typical of this source (Grisé et al. 2010), and while the variability properties of the radio core are not currently known, the triple-radio structure implies repeated jet emission (Cseh et al. 2014), broadly similar to SS433. However, as the X-ray emission from SS433 is thought to arise through plasma collisions within the jet, it may be more likely that the bremsstrahlung emission would scale with the kinetic power, $L_{\rm kin}$, of the jet instead, and $L_{\rm brems}/L_{\rm kin}$ may therefore be a more appropriate quantity to compare. Unfortunately neither SS433 or Holmberg II X-1 have robust constraints for $L_{\rm kin}$ at the time of writing (Marshall et al. 2013; Cseh et al. 2014), so we are not currently able to meaningfully assess whether these systems are similar in this regard.

Although it is therefore difficult to exclude the SS433-like jet interpretation, high accretion rate Galactic BHBs in the very high state exhibit steep ($\Gamma \sim 2.5$) high-energy power-law emission that can extend up to ∼MeV energies (e.g., Tomsick et al. 1999; Remillard & McClintock 2006). We therefore favor a similar interpretation for Holmberg II X-1, in which the high-energy emission is a power-law tail to the thermal continuum. The smooth nature of the high-energy spectrum and the transition from the hotter blackbody component to the hard excess probably also supports this interpretation over one invoking two essentially unrelated emission components. The likely origin of this power-law tail is Comptonization by a hot (or even non-thermal) coronal plasma. This implies that even though the 3–10 keV emission can formally be modeled with an optically thick COMPTT component, it is not physically associated with the Comptonizing corona. Therefore the thermal continuum likely arises from a high Eddington accretion disk (e.g., Poutanen et al. 2007; Middleton et al. 2011; Miller et al. 2014).

The physical nature of the soft blackbody component remains uncertain. Given the lack of strong variability between our observations we cannot differentiate between interpretations invoking disk emission, e.g., the "patchy disk" scenario recently proposed by Miller et al. (2014) in which the surface of the accretion disk is inhomogeneous, with a variety of hot patches embedded across a range of radii within a cooler surrounding medium, resulting in a more complex temperature profile than predicted by simple disk models) or emission from an optically thick wind (e.g., Middleton et al. 2015).

For the accretion disk case, the relative normalizations (N) of the DISKBB and DISKPBB models used for the continuum below 10 keV can in principle provide information on the emitting area of these components, as $N \propto R_{\rm in}^2/f_{\rm col}^4$ (where $R_{\rm in}$ is the inner radius of the disk and $f_{\rm col} = T_{\rm col}/T_{\rm eff}$ is the color correction factor relating the observed "color" temperature to the effective blackbody temperature at the midplane of the disk, accounting for e.g., the effects of scattering in the disk atmosphere on the latter). With the power-law (SIMPL) model for the high-energy emission, we find $N_{\rm cool} = 110^{+80}_{-60}$ (for DISKBB) and $N_{\rm hot} = 1.0^{+1.0}_{-0.5} \times 10^{-2}$ (for DISKPBB), implying relative emitting areas of $A_{\rm hot}/A_{\rm cool} \sim 10^{-4}$ (or, alternatively, relative sizes of $R_{\rm hot}/R_{\rm cool} \sim 10^{-2}$), assuming the same atmospheric correction for both.

This is very similar to the results obtained by Miller et al. (2014) for NGC 1313 X-1 and implies a much smaller emitting area for the hotter component. In the case of the DISKPBB component, the statistical uncertainty on the normalization is driven by a mild degeneracy with the radial temperature index (higher values of p give larger normalizations). However, for the thin disk scenario ($p = 0.75$) the normalization is only larger by a factor of ∼2, so this degeneracy will not significantly influence the general conclusion regarding the relative emitting areas. The relative atmospheric corrections for the two components is probably a more important issue in this regard. Shimura & Takahara (1995) find $f_{\rm col} = 1.7$ for the disk dominated high/soft state, but it is likely to vary outside of this accretion regime (see Reynolds & Miller 2013; Salvesen et al. 2013). Although we do not know $f_{\rm col}$, and it is entirely possible (if not likely) that it would be different for the hotter and cooler blackbody components, meaning the quantitative value of their relative emitting areas remains highly uncertain, it would take an extreme difference in $f_{\rm col}$ (i.e., a factor of ∼10) to reverse the conclusion about their relative areas.

For the wind model, deviations from the disk geometry assumed in the simple models used here would result in some additional correction for the area inferred, and one cannot formally define $f_{\rm col}$ in the same manner, as the wind would not have a mid-plane temperature. However, conceptually similar atmospheric corrections would still need to be accounted for, and these differences to the accretion disk case discussed above are also unlikely to be large enough to reverse the conclusion that the hotter component has a smaller emitting area than the cooler component.

This is consistent with both the patchy disk and disk/wind models. In the former, the hotter blackbody component arises from small patches that are hotter than their surroundings within an inhomogeneous disk and in the latter the hotter component arises from the inner disk and the cooler component arises from a disk wind launched at a larger radius. Further broadband observations that robustly constrain the relative evolution of the different emission components are required to differentiate between these interpretations. We may even find that both patchy accretion disks and large-scale disk winds contribute significantly to the osberved spectrum, as the presence of one does not necessarily exclude the other.

Finally, our 2013 campaign cannot constrain the metallicity of the absorbing medium toward Holmberg II X-1 (see Section 4). We note that if the metallicity of this absorbing material is close to solar, as suggested by the work of Goad et al. (2006) and Winter et al. (2007), it is significantly in excess of the metallicity inferred for the Holmberg II galaxy as a whole by Egorov et al. (2013). If confirmed, this would support a scenario in which the explosive event in which Holmberg II X-1 was formed enriched its local environment, resulting in a significantly enhanced local metallicity. Observations with the microcalorimeter due to fly on *Astro-H* (Takahashi et al. 2012) should have sufficient sensitivity and spectral resolution to accurately constrain both the oxygen and iron edges associated with the neutral absorber and robustly address the metallicity of the absorbing medium.

The authors would like to thank the referee for the positive feedback, which helped improve the clarity of the final manuscript. M.B. and D.B. acknowledge financial support from the French Space Agency (CNES). This research has made use of data obtained with *NuSTAR*, a project led by Caltech, funded by NASA and managed by NASA/JPL and has utilized the NUSTARDAS software package, jointly developed by the ASDC (Italy) and Caltech (USA). This research has also made use of data obtained with *XMM-Newton*, an ESA science mission with instruments and contributions directly funded by ESA Member States, and with *Suzaku*, a collaborative mission between the space agencies of Japan (JAXA) and the USA (NASA).

Facilites: NuSTAR, *XMM*, *Suzaku*.

REFERENCES

Abramowicz, M. A., Czerny, B., Lasota, J. P., & Szuszkiewicz, E. 1988, ApJ, 332, 646
Arnaud, K. A. 1996, in ASP Conf. Ser. 101, Astronomical Data Analysis Software and Systems V, ed. G. H. Jacoby, & J. Barnes (San Francisco, CA: ASP), 17
Bachetti, M., Harrison, F. A., Walton, D. J., et al. 2014, Natur, 514, 202
Bachetti, M., Rana, V., Walton, D. J., et al. 2013, ApJ, 778, 163
Begelman, M. C., King, A. R., & Pringle, J. E. 2006, MNRAS, 370, 399
Berghea, C. T., Dudik, R. P., Weaver, K. A., & Kallman, T. R. 2010, ApJ, 708, 364
Brenneman, L. W., Madejski, G., Fuerst, F., et al. 2014, ApJ, 788, 61
Caballero-García, M. D., & Fabian, A. C. 2010, MNRAS, 402, 2559
Cseh, D., Kaaret, P., Corbel, S., et al. 2014, MNRAS, 439, L1
Dotan, C., & Shaviv, N. J. 2011, MNRAS, 413, 1623
Egorov, O. V., Lozinskaya, T. A., & Moiseev, A. V. 2013, MNRAS, 429, 1450
Farrell, S. A., Webb, N. A., Barret, D., Godet, O., & Rodrigues, J. M. 2009, Natur, 460, 73
Feng, H., & Kaaret, P. 2009, ApJ, 696, 1712
Feng, H., & Soria, R. 2011, NAR, 55, 166
Gladstone, J. C., Roberts, T. P., & Done, C. 2009, MNRAS, 397, 1836
Goad, M. R., Roberts, T. P., Reeves, J. N., & Uttley, P. 2006, MNRAS, 365, 191
Grisé, F., Kaaret, P., Feng, H., Kajava, J. J. E., & Farrell, S. A. 2010, ApJL, 724, L148
Harrison, F. A., Craig, W. W., Christensen, F. E., et al. 2013, ApJ, 770, 103
Jansen, F., Lumb, D., Altieri, B., et al. 2001, A&A, 365, L1
Kaaret, P., Ward, M. J., & Zezas, A. 2004, MNRAS, 351, L83
Kajava, J. J. E., Poutanen, J., Farrell, S. A., Grisé, F., & Kaaret, P. 2012, MNRAS, 422, 990
Kalberla, P. M. W., Burton, W. B., Hartmann, D., et al. 2005, A&A, 440, 775
Karachentsev, I. D., Dolphin, A. E., Geisler, D., et al. 2002, A&A, 383, 125
King, A. R., Davies, M. B., Ward, M. J., Fabbiano, G., & Elvis, M. 2001, ApJL, 552, L109
Liu, J.-F., Bregman, J. N., Bai, Y., Justham, S., & Crowther, P. 2013, Natur, 503, 500
Lopez, L. A., Marshall, H. L., Canizares, C. R., Schulz, N. S., & Kane, J. F. 2006, ApJ, 650, 338
Madsen, K. K., Harrison, F. A., Markwardt, C., et al. 2015, arXiv:1504.01672
Marshall, H. L., Canizares, C. R., Hillwig, T., et al. 2013, ApJ, 775, 75
Marshall, H. L., Canizares, C. R., & Schulz, N. S. 2002, ApJ, 564, 941
Middleton, M. J., Heil, L., Pintore, F., Walton, D. J., & Roberts, T. P. 2015, MNRAS, 447, 3243
Middleton, M. J., Miller-Jones, J. C. A., Markoff, S., et al. 2013, Natur, 493, 187
Middleton, M. J., Roberts, T. P., Done, C., & Jackson, F. E. 2011, MNRAS, 411, 644
Miller, J. M., Bachetti, M., Barret, D., et al. 2014, ApJL, 785, L7
Miller, J. M., Raymond, J., Fabian, A. C., et al. 2004, ApJ, 601, 450
Miller, J. M., Walton, D. J., King, A. L., et al. 2013, ApJL, 776, L36
Miller-Jones, J. C. A., Migliari, S., Fender, R. P., et al. 2008, ApJ, 682, 1141
Mineshige, S., Hirano, A., Kitamoto, S., Yamada, T. T., & Fukue, J. 1994, ApJ, 426, 308
Mitsuda, K., Bautz, M., Inoue, H., et al. 2007, PASJ, 59, 1
Mitsuda, K., Inoue, H., Koyama, K., et al. 1984, PASJ, 36, 741
Motch, C., Pakull, M. W., Soria, R., Grisé, F., & Pietrzyński, G. 2014, Natur, 514, 198
Mukherjee, E. S., Walton, D. J., Bachetti, M., et al. 2015, arXiv:1502.01764
Orosz, J. A. 2003, in IAU Symp. 212, A Massive Star Odyssey: From Main Sequence to Supernova, ed. K. van der Hucht, A. Herrero, & C. Esteban (San Francisco, CA: ASP), 365
Pasham, D. R., Strohmayer, T. E., & Mushotzky, R. F. 2014, Natur, 513, 74
Poutanen, J., Lipunova, G., Fabrika, S., Butkevich, A. G., & Abolmasov, P. 2007, MNRAS, 377, 1187
Rana, V., Harrison, F. A., Bachetti, M., et al. 2015, ApJ, 799, 121
Remillard, R. A., & McClintock, J. E. 2006, ARA&A, 44, 49
Reynolds, M. T., & Miller, J. M. 2013, ApJ, 769, 16
Roberts, T. P. 2007, Ap&SS, 311, 203
Salvesen, G., Miller, J. M., Reis, R. C., & Begelman, M. C. 2013, MNRAS, 431, 3510
Servillat, M., Farrell, S. A., Lin, D., et al. 2011, ApJ, 743, 6
Shakura, N. I., & Sunyaev, R. A. 1973, A&A, 24, 337
Shimura, T., & Takahara, F. 1995, ApJ, 445, 780
Steiner, J. F., Narayan, R., McClintock, J. E., & Ebisawa, K. 2009, PASP, 121, 1279
Stobbart, A.-M., Roberts, T. P., & Wilms, J. 2006, MNRAS, 368, 397
Sutton, A. D., Roberts, T. P., Walton, D. J., Gladstone, J. C., & Scott, A. E. 2012, MNRAS, 423, 1154
Swartz, D. A., Soria, R., Tennant, A. F., & Yukita, M. 2011, ApJ, 741, 49
Takahashi, T., Mitsuda, K., Kelley, R., et al. 2012, Proc. SPIE, 8443, 84431Z
Titarchuk, L. 1994, ApJ, 434, 570
Tomsick, J. A., Kaaret, P., Kroeger, R. A., & Remillard, R. A. 1999, ApJ, 512, 892
Verner, D. A., Ferland, G. J., Korista, K. T., & Yakovlev, D. G. 1996, ApJ, 465, 487

Walton, D. J., Fuerst, F., Harrison, F., et al. 2013a, ApJ, 779, 148
Walton, D. J., Gladstone, J. C., Roberts, T. P., et al. 2011a, MNRAS, 414, 1011
Walton, D. J., Harrison, F. A., Bachetti, M., et al. 2015, ApJ, 799, 122
Walton, D. J., Harrison, F. A., Grefenstette, B. W., et al. 2014, ApJ, 793, 21
Walton, D. J., Miller, J. M., Harrison, F. A., et al. 2013b, ApJL, 773, L9
Walton, D. J., Roberts, T. P., Mateos, S., & Heard, V. 2011b, MNRAS, 416, 1844
Wilms, J., Allen, A., & McCray, R. 2000, ApJ, 542, 914
Winter, L. M., Mushotzky, R. F., & Reynolds, C. S. 2007, ApJ, 655, 163
Zampieri, L., & Roberts, T. P. 2009, MNRAS, 400, 677